Wavelet Analysis of a Blade Tip-Leakage Flow

Jérôme Boudet[*]
École Centrale de Lyon, 69134 Ecully, France
Marc C. Jacob[†]
ISAE-SUPAERO, 31400 Toulouse, France
and
Joëlle Caro,[‡] Emmanuel Jondeau,[‡] and Bo Li[§]
École Centrale de Lyon, 69134 Ecully, France

I. Introduction

IN TURBOMACHINES (shrouded fans, compressors, turbines, etc.), clearances are located between vane or blade tips and end walls (hub or casing) in order to allow a relative motion. Such gaps result in a strong leakage flow, driven by the pressure difference and affected by the relative wall motion. When it interacts with the main flow, the leakage jet produces a streamwise vortex, referred to as the tip-leakage vortex (TLV) and possibly other vortices (e.g., counter-rotating vortices) [1]. This is sketched in Fig. 1. At a high Reynolds number, turbulence is transported and produced in this vortical flow, and broadband noise is generated. Similar flows also develop on aircraft wings, around the clearances located between the flap sides and the enfolding static airframe components.

Detailed experimental characterizations of the tip-leakage flow in a blade cascade have been carried out by Muthanna and Devenport [2] and Wang and Devenport [3], with stationary and moving end walls. This extensive work has been used as reference for a large-eddy simulation (LES) performed by You et al. [4]. LES uses a direct description of the largest and most energetic turbulent eddies, which enables a detailed analysis of the turbulent dynamics. More recently, Pogorelov et al. [5] presented LES simulations of a five-blade rotor, with a particular attention paid to the tip-leakage flow.

In the present paper, a rather simple configuration is considered: a single airfoil, between two end plates, with a clearance at the lower end. This simplicity enabled Jacob et al. [6,7] to carry out a detailed experimental characterization, on both aerodynamics and acoustics. A zonal large-eddy simulation was also performed on the same configuration and compared very favorably to the experiment, as shown by Boudet et al. [8,9] on mean flow, Reynolds stresses, and spectra. In both the experiment and the simulation, a broad hump was observed on pressure spectra at tip, around 1.3 kHz, within the frequency range in which the tip leakage has a significant noise contribution (0.7–7 kHz). The objective of the present paper is to exploit the high-fidelity simulation for a detailed analysis of this unsteadiness in the tip-leakage flow, around 1.3 kHz.

II. Configuration and Numerical Parameters

A. Experimental Configuration

The experimental configuration is constituted by a single airfoil set in the potential core of a jet, between two end plates. As sketched on Fig. 2, a clearance is arranged between the airfoil and the lower (casing) plate. The chord length is $c = 0.2$ m, the upstream velocity is $U_0 = 70$ m/s, which yields a Reynolds number $Re_c = 9.3 \times 10^5$ and a Mach number $M = 0.2$. The clearance height is $h = 0.01$ m, and the freestream rms velocity fluctuation at inflow is $0.5\% \, U_0$. In a previous version of the experiment [10], the angle of attack was 15 deg (± 0.5 deg), but the experimental results used in the present paper have been obtained during a more recent campaign, in which the angle of attack had to be set to 16.5 deg (± 0.5 deg) in order to recover the same airfoil loading as the original experiment. The details of the experimental configuration and an analysis of the experimental results are presented by Jacob et al. [6,7].

B. Zonal Large-Eddy Simulation

The simulation uses a zonal approach. It enables defining a region of interest (the tip clearance region in the present case), in which large-eddy simulation is used for a direct description of the most energetic turbulent eddies. In the other regions, a Reynolds-averaged Navier–Stokes (RANS) approach is used in order to reduce the computational cost. The zonal decomposition of the domain is defined by the user, through a weighting function of the LES and RANS eddy viscosities. The lateral boundaries of the LES zones need to be approximately positioned along mean stream surfaces. The formulation of the zonal approach is explained in details by Boudet et al. [11]. In Fig. 3, instantaneous contours of velocity are shown on a plane just above the clearance, together with the zonal decomposition of the computational domain for the present simulation. The region of higher velocities corresponds to the tip clearance jet, and the velocity fluctuations downstream of the suction side indicate the TLV location. The main jet is deviated by the airfoil, and this deviation has to be taken into account to reproduce the airfoil loading, as discussed by Moreau et al. [12]. At this spanwise position, near the tip, the LES zone corresponds approximately to the interior of the jet. Along the span, it extends over $5h$ above the lower end plate. This zonal decomposition has been defined based upon a preliminary RANS computation. Most of the jet shear layers and the outer region at rest are simulated with RANS in order to alleviate the computational cost. On the lateral boundaries of the LES zone, where the flow is roughly tangent to the surface, no specific treatment is done; eddy viscosity evolves smoothly from the LES value to the RANS value, and vice versa, controlled by the weighting function. However, turbulent quantities need to be imposed at the inflow of the LES zone; a flat-plate boundary layer is simulated with LES over a limited width and duplicated laterally to feed the LES zone. The duplication is sketched by the arrows in Fig. 3. The width of the incoming boundary layer domain is $1.4h$, corresponding to 12 times the momentum thickness at $0.5c$ upstream of the blade leading edge. At the inflow, turbulence outside of the boundary layer is neglected. Concerning the models, LES uses the shear-improved Smagorinsky model from Lévêque et al. [13], and RANS uses the Wilcox $k - \omega$ model [14].

The solver *Turb'Flow* is an in-house finite-volume code for multiblock structured grids. The inviscid flux interpolation uses a four-point centered scheme. In the LES zone, a fourth-order artificial
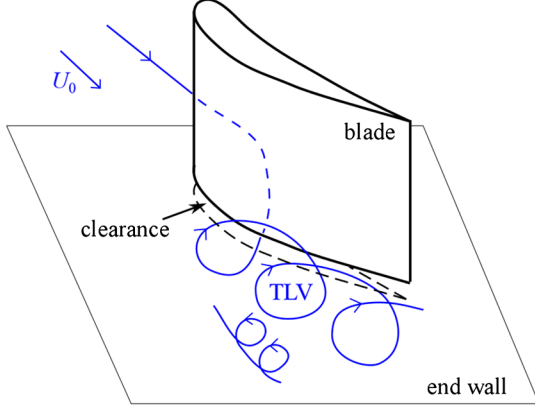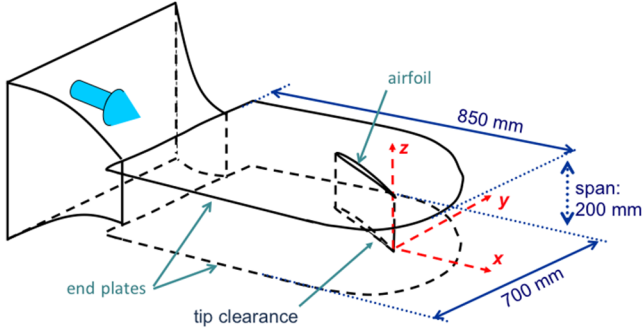
Fig. 1 Sketch of a tip-clearance flow.

Fig. 2 Experimental configuration. The origin of the coordinate system is on the blade tip/trailing-edge corner, with $z \leq 0$ in the clearance.
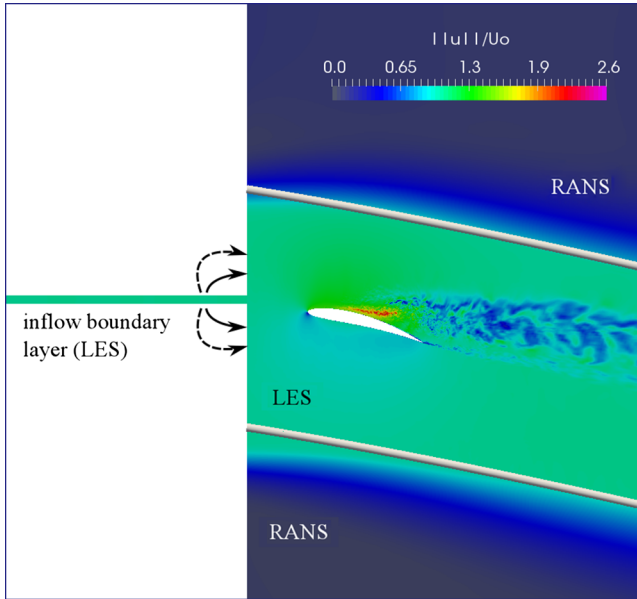

Fig. 3 Instantaneous contours of the velocity magnitude around the airfoil at $z = 0.5h$, with indication of the LES and RANS zones (the separation between the zones is marked by a thick gray line).

viscosity is used (definition in Boudet et al. [15]), with a coefficient evolving smoothly from 0.003 at the lower end-wall, up to 0.02 above. Increased numerical viscosity is used in peripheral regions. The viscous flux interpolation uses a two-point centered scheme. Time marching is explicit, with a three-step Runge–Kutta scheme and a time step of $5.6 \times 10^{-6} c/U_0$. Because the simulation was initiated before the second test campaign, the original angle of attack (15 deg) was chosen. After convergence, results were stored every
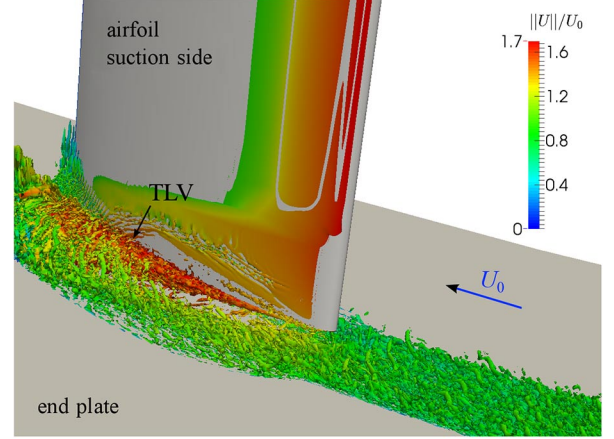

Fig. 4 3D instantaneous view of the zonal LES simulation. Isosurface of Q criterion, colored by the velocity magnitude.

3000 iterations over more than $10 \cdot c/U_0$ (instead of $6 \cdot c/U_0$ in [8]), and flow statistics were computed on the fly.

In the LES zone, the grid resolution is $\Delta x^+ < 80$ (streamwise), $\Delta y^+ < 1.5$ (wall normal), and $\Delta z^+ < 30$ (cross-stream), for a full LES resolution of the boundary layers. The computational domain extends over $29c$ axially, $37c$ laterally, and $1c$ spanwise, with the end plates extending over the whole domain. The total number of grid points is about 150×10^6, distributed over 524 structured blocks for parallel computing. More details about the computation and its validation against experimental data can be found in [8,9].

An instantaneous three-dimensional view of the simulated flowfield is shown in Fig. 4. The turbulent eddies in the incoming boundary layer are shown to interact with the leakage flow. The TLV vortex also appears on the figure and is characterized by higher velocities.

III. Wavelet Analysis: Methodology

In both the experiment [6,7] and the simulation [8,9], a broad hump was observed in near-field spectra at the airfoil tip, around 1.3 kHz. Moreover, its frequency range, which extends over more than two octave bands, is located within that of the tip-leakage noise (0.7–7 kHz), which makes it particularly interesting. In the present section, a methodology is set up to identify the flow mechanism at the origin of this unsteadiness.

A time trace of the pressure felt by probe 46 is plotted in Fig. 5. Probe 46 is located on the pressure side at $77.5\%c$, 1.5 mm above the tip edge. Large oscillations are observed, with a time scale of order 10^{-3} s, which is consistent with the frequency 1.3 kHz. The objective
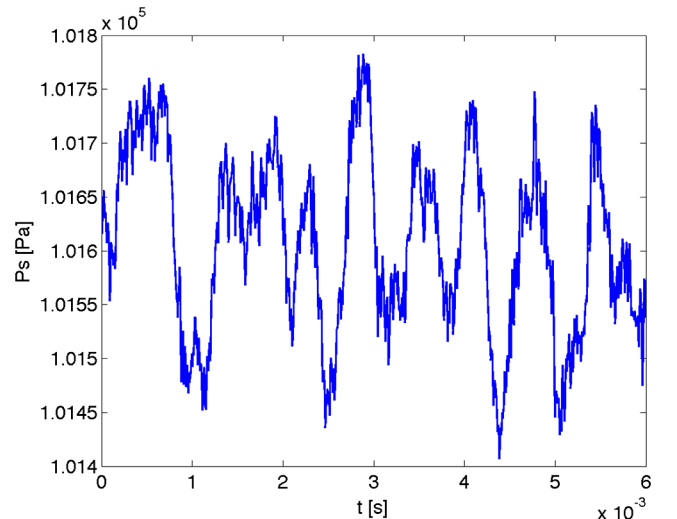

Fig. 5 Portion of the time trace of pressure, on probe 46 (pressure side, $77.5\%c$ and 1.5 mm above the blade tip), from the simulation.

is to detect these events and identify the flow features that are correlated with them. Since these events are unevenly spaced and show variations in their duration, wavelet analysis appears to be promising if not more appropriate than classical Fourier analysis to identify such intermittent events. The detection of flow events with wavelets is a well-known topic of research and has already been applied to the present configuration by Camussi et al. [16] on the experimental results of the first campaign. The present paper is not focused on the mathematics of the wavelet technique but merely relies on an elementary wavelet decomposition, with the objective to identify the unsteady flow phenomena in the tip region. Compared to the paper of Camussi et al., the novelty of the present investigation lies in the use of validated numerical results, which provide a three-dimensional high-frequency description of the flow, particularly of interest for the detection of local flow phenomena.

The classical wavelet known as Mexican hat is used to decompose the pressure signal from probe 46. The continuous wavelet transform of the full-length signal is carried out with MATLAB® (R2012b), and the resulting scalogram is plotted in Fig. 6. This figure shows the time evolution of the energy content associated with the main unsteady flow events. These events are not identified through a classical Fourier time-frequency analysis but by the time scales of the wavelets they are associated with. A number of energetic events are observed around the wavelet scale $2 \cdot 10^{-4}$ s. Given the shape of the Mexican hat wavelet (for which the scale corresponds to the abscissa distance between the maximum and the x intercept), this scale value can be associated with a period of $8 \cdot 10^{-4}$ s, i.e., a frequency of ~1.3 kHz. These events correspond to the large oscillations observed in Fig. 5 and to the spectrum hump around 1.3 kHz. In the scalogram (Fig. 6), the maxima that satisfy the following rules are marked with symbols: the frequency between 0.5×1.3 and 2×1.3 kHz, and the energy superior to 20% of the scalogram maximum. These maxima of energy correspond to either local pressure maxima or local pressure minima. The crosses indicate the local pressure maxima (positive decomposition coefficient), and the circles indicate the local pressure minima (negative decomposition coefficient). These extrema are used to locate the events. Considering their distribution in the scalogram, the following comments can be drawn. The events do not occur regularly in time but by packets of variable duration, during which minima and maxima of pressure alternate. The scale of the events (and the associated frequency) is also variable, which can be related to the broad shape of the hump in the spectrum.

To isolate the flow phenomenon responsible for these events, a conditional average of the three-dimensional flow is carried out, triggered by the events marked in the scalogram of probe 46. This is expected to smooth out most of the turbulent fluctuations and bring
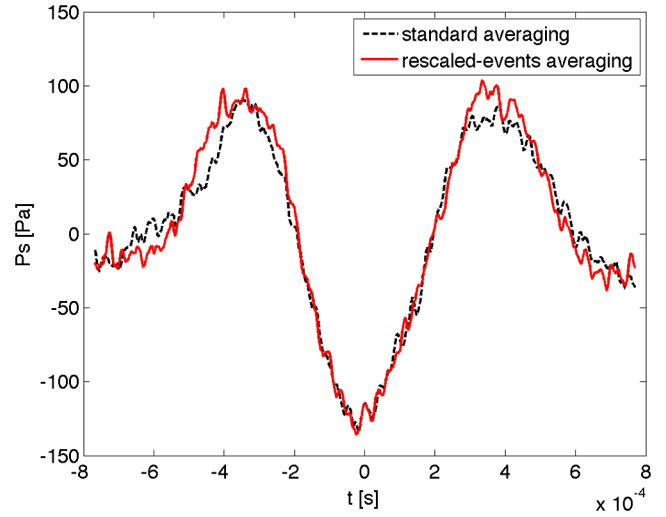
Fig. 7   Time trace of the mean event on probe 46.

out the unsteady phenomenon. The operation is first carried out on pressure probe 46 itself. Practically, we consider all the pressure minima in Fig. 6, we define time windows over one period on each side of the minima, and we average the different windows with each other. This yields the time trace of the mean event, as shown in Fig. 7. Two methods are tested for the average: the period is either assumed fixed (equal to $1/1300 \approx 8 \cdot 10^{-4}$ s) or calculated from the local scale value of the event ($4 \times$ scale). In the first method (standard averaging), the time scale of the windows is not altered, whereas in the second method (rescaled-events averaging), the instantaneous windows are rescaled to the reference period (equal to $1/1300 \approx 8 \cdot 10^{-4}$ s) before the average. The amplitude of the mean events in Fig. 7 is significant (≈ 250 Pa peak to peak) and comparable to that of the instantaneous events observed in Fig. 5. But the shape of the mean events is much smoother. These observations indicate there is a good repetition of the event shape in the instantaneous signal, and the averaging is effective. The rescaled-events averaging is slightly more effective, with a slightly larger amplitude of the mean event. The difference is moderate, but the methods are of similar complexity, and consequently the rescaled-events averaging is used for the rest of the study. To conclude this presentation of the conditional averaging procedure, one must notice the choice of the pressure minima as event centers is arbitrary. The whole procedure could be performed likewise by centering the events on the pressure maxima. Furthermore, Fig. 6 shows a good alternation of the minima and maxima. Consequently, even if the events are centered on the minima, the maxima can be detected by the lateral maxima of the wavelet, at an equivalent 180 deg phase shift.

IV.   Analysis of Unsteadiness at Tip

The conditional average controlled by the wavelet analysis of the probe signal is now applied to the whole three-dimensional (3D) unsteady flowfield. This process is expected to preserve the unsteady phenomenon associated with the events detected by probe 46, while smoothing out the other fluctuations. The 3D flow event is decomposed into 32 phases, from phase -180 deg (time $= -2 \times$ scale) to phase $+180$ deg (time $= 2 \times$ scale), with phase 0 deg corresponding to the minimum value of the probe event in Fig. 7. First, the location of the flow phenomenon in the 3D domain must be established. This is done by computing the velocity fluctuation intensity (VFI) of the conditional average

$$\text{VFI} = \frac{\sqrt{\langle u_{CA}'^2 + v_{CA}'^2 + w_{CA}'^2 \rangle / 3}}{U_0}$$

where $\langle \cdot \rangle$ is the time average and u_{CA}', v_{CA}', and w_{CA}' are the velocity fluctuations, from the conditionally averaged flow, over the phases -180 to 180 deg. The VFI distribution is analyzed in Fig. 8, on a
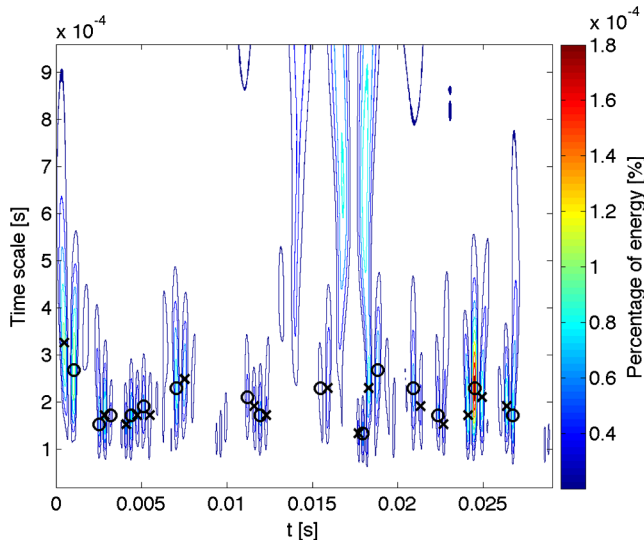

Fig. 6   Scalogram of the fluctuating pressure signal collected from probe 46. Crosses (x) indicate local pressure maxima and circles (o) indicate local pressure minima.
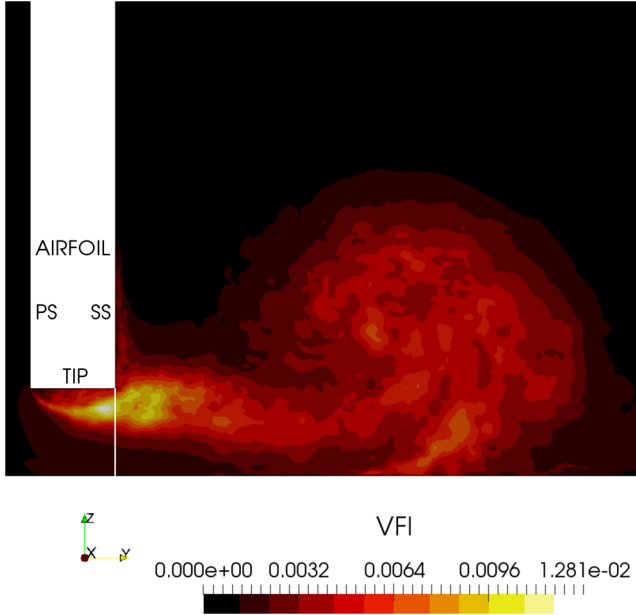
Fig. 8 VFI of the conditional average on a constant x plane at $79\%c$. The thin white line at the clearance outlet corresponds to the position of the velocity profiles in Fig. 9.

cutting plane at constant x positioned through the maximum of VFI. The most intense fluctuations occur in the aft part of the airfoil (constant x plane at $79\%c$), near the probe that has been used to detect and define the event (probe 46 is at $77.5\%c$). The VFI is the most intense around the suction-side/tip corner, in the shear zone between the leakage flow and the main flow. Fluctuations are also observed in the TLV, but with a smaller intensity.

To characterize the flow phenomenon associated with this event, profiles of the conditionally averaged y-velocity component v_{CA}/U_0 are plotted in Fig. 9 on a line at the clearance outlet (position shown in Fig. 8). These profiles are characterized by the intense leakage flow at low $\Delta z/h$ ($v_{CA}/U_0 \approx 0.8$) and backflow above ($v_{CA}/U_0 < 0$). The backflow corresponds to a tip separation. Interestingly, this separation is shown to oscillate, in correlation with the event phase: the separation is thick at $\theta = -180$ deg, it progressively reduces until $\theta = 0$ deg, and it thickens again for positive θ. These results indicate the event observed on probe 46, associated with the spectrum hump around 1.3 kHz, corresponds to an unsteady tip separation. The corresponding Strouhal number, calculated with U_0 and the tip-gap height (of the same order as the airfoil thickness in this region), is
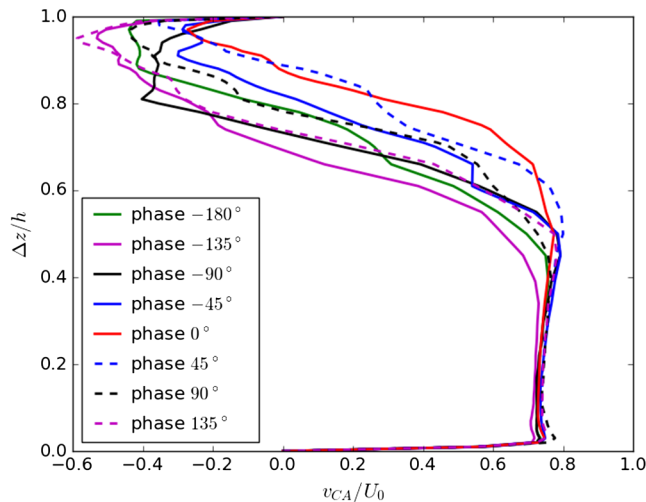

Fig. 9 Conditional average of the flow: profiles of v_{CA}/U_0 in the constant x plane at $79\%c$ on the suction-side outlet of the clearance (extraction line shown in Fig. 8), for different phases.

$St = 0.19$. This order of magnitude is compatible with a vortex shedding process.

V. Conclusions

The unsteadiness of a simplified tip-leakage flow has been analyzed in a zonal LES simulation, previously validated against experimental results. Attention has been focused around a specific frequency (1.3 kHz, or $St = 0.19$), at which a hump was previously observed in spectra at the tip.

A methodology has been proposed to identify the unsteady phenomenon related to this frequency. It uses wavelets to 1) detect the irregular occurrences of the events and 2) define a conditional average of the 3D flowfield. Fluctuations in the time scales of the events have been captured by the methodology and relate to the broad nature of the spectrum hump. Finally, the analysis of the conditionally averaged flow allowed to locate the origin of the events and to characterize the physical phenomenon as an unsteady separation at the blade tip.

The present methodology can be used to locate and identify intermittent flow phenomena around a given frequency. In the present configuration, it allowed discerning a blade tip separation that contributes to the far-field noise.

References

[1] Lakshminarayana, B., *Fluid Dynamics and Heat Transfer of Turbomachinery*, Wiley, Hoboken, NJ, 1996.
[2] Muthanna, C., and Devenport, W. J., "Wake of a Compressor Cascade with Tip Gap, Part 1: Mean Flow and Turbulence Structure," *AIAA Journal*, Vol. 42, No. 11, 2004, pp. 2320–2331.
doi:10.2514/1.5270
[3] Wang, Y., and Devenport, W. J., "Wake of a Compressor Cascade with Tip Gap, Part 2: Effects of Endwall Motion," *AIAA Journal*, Vol. 42, No. 11, 2004, pp. 2332–2340.
doi:10.2514/1.5272
[4] You, D., Wang, M., Moin, P., and Mittal, R., "Large-Eddy Simulation Analysis of Mechanisms for Viscous Losses in a Turbomachinery Tip-Clearance Flow," *Journal of Fluid Mechanics*, Vol. 586, Sept. 2007, pp. 177–204.
doi:10.1017/S0022112007006842
[5] Pogorelov, A., Meinke, M., and Schröder, W., "Cut-Cell Method Based Large-Eddy Simulation of Tip-Leakage Flow," *Physics of Fluids*, Vol. 27, No. 7, 2015, Paper 075106.
doi:10.1063/1.4926515
[6] Jacob, M. C., Jondeau, E., and Li, B., "Time-Resolved PIV Measurements of a Tip Leakage Flow," *International Journal of Aeroacoustics*, Vol. 15, Nos. 6–7, 2016, pp. 662–685.
doi:10.1177/1475472X16659384
[7] Jacob, M., Jondeau, E., Li, B., and Boudet, J., "Tip-Leakage Flow: Advanced Measurements and Analysis," *22nd AIAA/CEAS Aeroacoustics Conference*, AIAA Paper 2016-2823, 2016.
doi:10.2514/6.2016-2823
[8] Boudet, J., Caro, J., Li, B., Jondeau, E., and Jacob, M., "Zonal Large-Eddy Simulation of a Tip Leakage Flow," *International Journal of Aeroacoustics*, Vol. 15, Nos. 6–7, 2016, pp. 646–661.
doi:10.1177/1475472X16659215
[9] Boudet, J., Li, B., Caro, J., Jondeau, E., and Jacob, M., "Tip-Leakage Flow: A Detailed Simulation with a Zonal Approach," *22nd AIAA/CEAS Aeroacoustics Conference*, AIAA Paper 2016-2824, 2016.
doi:10.2514/6.2016-2824
[10] Jacob, M. C., Grilliat, J., Camussi, R., and Caputi Gennaro, G., "Aeroacoustic Investigation of a Single Airfoil Tip Leakage Flow," *International Journal of Aeroacoustics*, Vol. 9, No. 3, 2010, pp. 253–272.
doi:10.1260/1475-472X.9.3.253
[11] Boudet, J., Cahuzac, A., Kausche, P., and Jacob, M., "Zonal Large-Eddy Simulation of a Fan Tip-Clearance Flow, with Evidence of Vortex

Wandering," *Journal of Turbomachinery*, Vol. 137, No. 6, 2015, Paper 061001.
doi:10.1115/1.4028668

[12] Moreau, S., Henner, M., Iaccarino, G., Wang, M., and Roger, M., "Analysis of Flow Conditions in Freejet Experiments for Studying Airfoil Self-Noise," *AIAA Journal*, Vol. 41, No. 10, 2003, pp. 1895–1905.
doi:10.2514/2.1905

[13] Lévêque, E., Toschi, F., Shao, L., and Bertoglio, J. P., "Shear-Improved Smagorinsky Model for Large-Eddy Simulation of Wall-Bounded Turbulent Flows," *Journal of Fluid Mechanics*, Vol. 570, Jan. 2007, pp. 491–502.
doi:10.1017/S0022112006003429

[14] Wilcox, D., "Reassessment of the Scale-Determining Equation for Advanced Turbulence Models," *AIAA Journal*, Vol. 26, No. 11, 1988, pp. 1299–1310.
doi:10.2514/3.10041

[15] Boudet, J., Monier, J.-F., and Gao, F., "Implementation of a Roughness Element to Trip Transition in Large-Eddy Simulation," *Journal of Thermal Science*, Vol. 24, No. 1, 2015, pp. 30–36.
doi:10.1007/s11630-015-0752-8

[16] Camussi, R., Grilliat, J., Caputi-Gennaro, G., and Jacob, M. C., "Experimental Study of a Tip Leakage Flow: Wavelet Analysis of Pressure Fluctuations," *Journal of Fluid Mechanics*, Vol. 660, Oct. 2010, pp. 87–113.
doi:10.1017/S0022112010002570